HOKKAIDO UNIVERSITY

Title	Nanocrack Formation in Hematite through the Dehydration of Goethite and the Carbon Infiltration from Biotar
Author(s)	Kashiwaya, Yoshiaki; Akiyama, Tomohiro
Citation	Journal of Nanomaterials, 2010, 235609 https://doi.org/10.1155/2010/235609
Issue Date	2010
Doc URL	https://hdl.handle.net/2115/44165
Rights(URL)	https://creativecommons.org/licenses/by/2.0/
Type	journal article
File Information	JN2010_235609.pdf

Research Article

Nanocrack Formation in Hematite through the Dehydration of Goethite and the Carbon Infiltration from Biotar

Yoshiaki Kashiwaya[1] and Tomohiro Akiyama[2]

[1] Depatment of Energy Science and Technology, Kyoto University, Sakyo-ku, Yoshida Honmachi, Kyoto 606-8501, Japan
[2] Center for Advanced Research of Energy Conversion Materials, Hokkaido University, kita 18, Nishi 8, Kita-ku 060-8072, Japan

Correspondence should be addressed to Yoshiaki Kashiwaya, kashiwaya@namihei.mtl.kyoto-u.ac.jp

The cracks in nano-order are generated and propagated when the combined water is released during the dehydration. If the nanopore can be utilized for a reaction site, the overall reaction can be extremely accelerated. On the other hand, it is well known that woody biomass is an attractive alternative fuel for the reduction of CO_2 emission. However, the process of biomass pyrolysis is disturbed by the tar which causes a clogging in gas tubing system. Hata et al. found that the tar was consumed almost 100% in the iron ore layer having nanocrack or nanopore. The nanocracks formed in hematite crystals after dehydration of goethite were about 4 nm in width, which is in excellent agreement with the result of BET measurement. When the carbon deposited from tar into the nanocracks, reduction reactions were occurred simultaneously. The deposited carbons completely infilled into the nanocracks and the void in the sample.

1. Introduction

It is well known that a woody biomass is an attractive alternative fuel for the reduction of CO_2 emission. We can easily produce a reducing gas and char from the pyrolysis of biomass; however, the biomass pyrolysis has a serious problem, that is, a sticky tar generates as a byproduct. The process of biomass pyrolysis is disturbed by the tar which causes a contamination in the inner wall of a reactor and a clogging in gas tubing system. To avoid these problems, high-temperature operation over 800°C, which corresponds to high energy consumption, is necessary.

Therefore, to use biomass effectively, the technology development of biomass pyrolysis at low temperature without tar generation is strongly required.

Under these circumstances, Hata et al. [1] reported the unique process named "Biotar ironmaking", which consisted of the formation of nanocrack or nanopore through the dehydration of goethite, and at the same time, the deposition of carbon into the crack (pore) from tar generated by the pyrolysis of wood biomass. They found that the reduction of iron oxide occurred simultaneously during carbon deposition from tar. Furthermore, the tar was consumed almost 100% in the iron ore layer, which was quite an important result for the utilization of wood biomass [2, 3].

On the other hand, effective use of low-grade limonite iron ore such as, Australian goethite for ironmaking can be a key technology for surmounting the recent increase of raw materials' cost.

However, due to the existence of combined water (CW), the goethite is difficult to use in the ironmaking process. In contrast, the dehydration of ore is physically interesting for the formation of pores or cracks in materials. For example, the cracks in nano-order are generated and propagated when the combined water is released during the dehydration [4–10]. If the nanopore can be utilized for a reaction site, the overall reaction can be extremely accelerated. However, the nanopores or nanocracks are not yet observed directly after dehydration of goethite. The increase of specific surface area was measured using BET (Brunaure-Emmett-Teller) method, which was an indirect evidence of submicron pores or cracks.
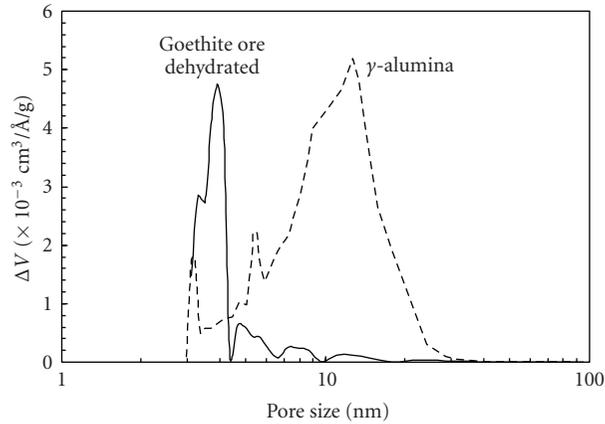
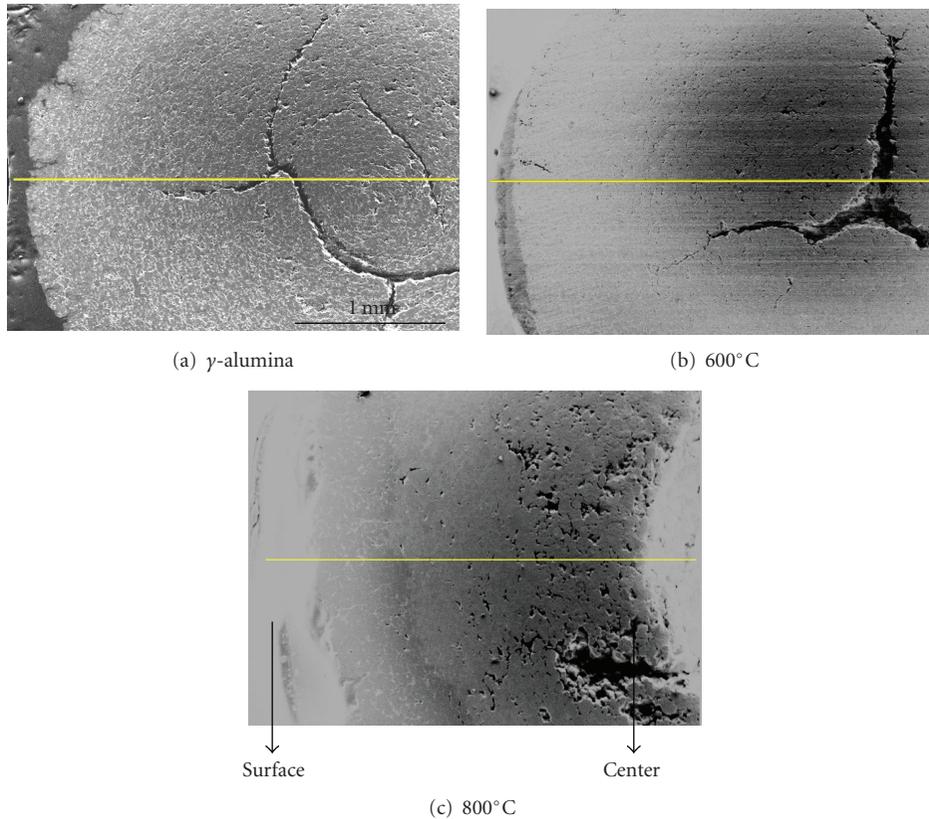FIGURE 1: Distributions of pore size in goethite ore and γ-alumina.

(a) γ-alumina

(b) 600°C

(c) 800°C

FIGURE 2: Cross section of SEM images of the γ-alumina before and after carbon deposition from tar.

In the present paper, we intended to clarify the shape and dimension of the crack or pore generated from the dehydration of goethite through the observations of high magnification using FE-SEM. Furthermore, the distribution and morphology of carbon deposited from tar were observed. Finally, a possible mechanism of carbon deposition from tar in the crack or pore together with the reduction of iron ore was presented.

2. Experimental

Experimental apparatus and procedure were the same as Hata et al. [1] used. The combined water (CW) of goethite iron ore was 9.02 mass% and total iron (T.Fe) was 57.2 mass%, whose removable oxygen was 24.58 mass%. The particle size of the sample was adjusted from 355 μm to 500 μm. The BET surface areas before and after dehydration
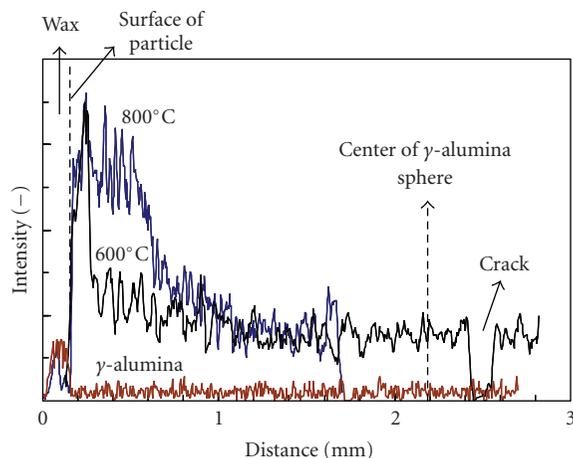
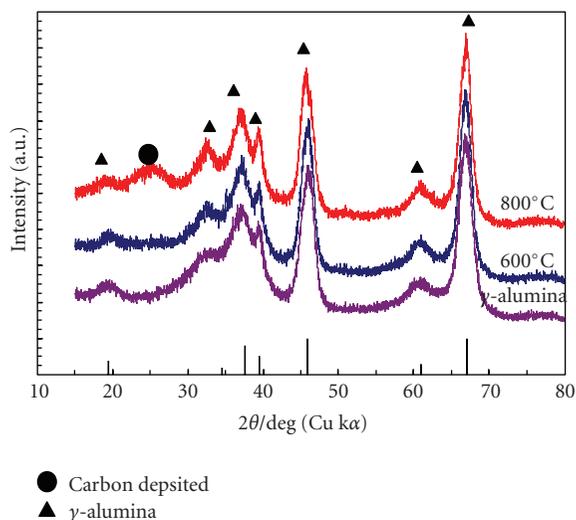Figure 3: Line analysis of carbon by EDS in the γ-Alumina with/without carbon deposited from tar.

● Carbon depsited
▲ γ-alumina

Figure 4: XRD results for the γ-alumina with/without carbon deposited from tar.

were 16.58 cm²/g and 74.90 cm²/g, respectively, (Table 1). The surface area after dehydration increased in 4.5 times, and the average pore size was about 4 nm [1]. If it was a round pore about 4 nm, it was expected that the surface energy of the pore should be quite high. Then, we expected that the pore in nano-order might be a kind of crack in nano-order. It is very important to observe the crack directly.

The goethite sample was heated under air atmosphere at 450°C and the CW was eliminated by the dehydration reaction completely. A pulverized pine tree was fed into the pyrolyzer at 600°C with 0.07 g/min. The generated tar flowed into the coking bed at 500°C, in which the ore sample of 3.0 g was set. Nitrogen gas of 200 cm³/min (STP) was flowed in the pyrolyzer and the coker.

γ-alumina sphere with 4 mm in diameter was also used for the comparison with iron ore, so that the carbon deposition from tar could be simulated without reduction reaction. The porosity of γ-alumina was about 79% and the

major pore size was around 10 nm, while the one of goethite ore after dehydration was around 4 nm (Figure 1).

3. Results and Discussions

3.1. Carbon Deposition in γ-Alumina. When carbon deposition occurred in an iron ore, reduction reaction will occur, more or less, simultaneously. In the case of this situation, a feature of carbon deposition from tar into a nanopore or crack cannot be understood. Then, a γ-alumina sphere with 4 mm in diameter was used instead of goethite ore. The carbon deposition experiments from tar were carried out at 600°C and 800°C. The cross sections of γ-alumina before and after experiments were compared in Figure 2, in which the right-hand side of photo corresponds to a center of particle and the left-hand side corresponds to the surface of particle. As the γ-alumina is not stable in a high temperature
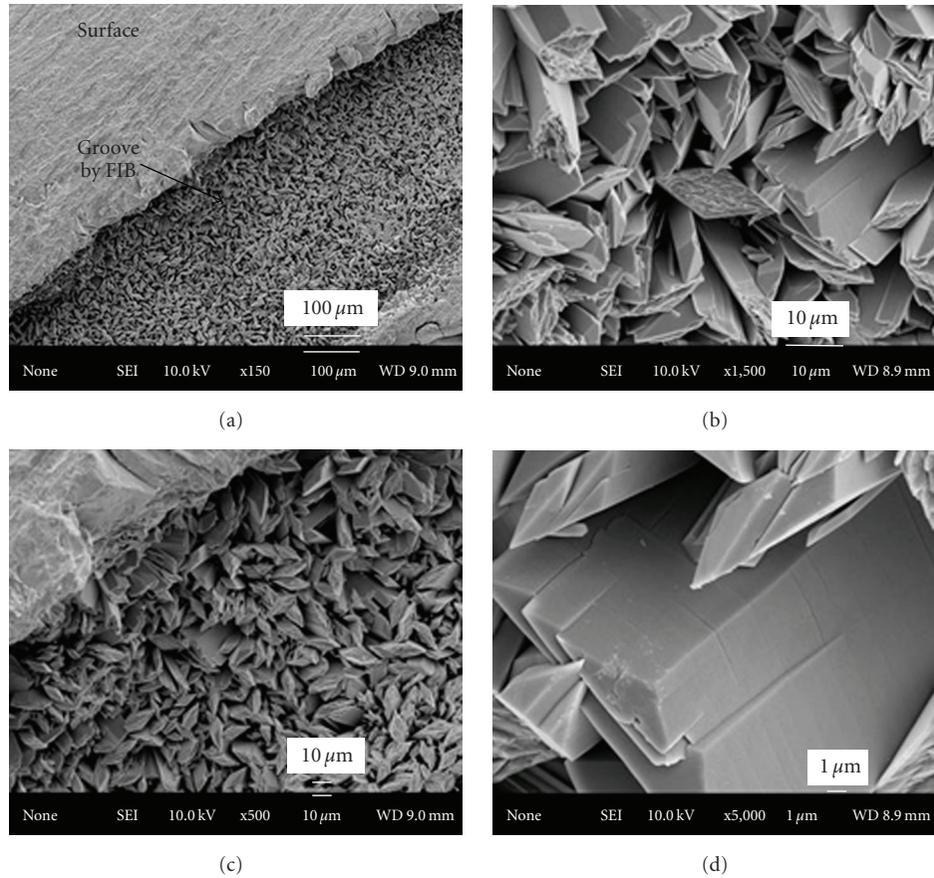
(a)

(b)

(c)

(d)

FIGURE 5: Microstructure of goethite dehydrated at 400°C.

TABLE 1: Goethite sample ore used in the experiments.

Sample ore	Particle size (μm)	CW (mass%)	T. Fe (mass%)	R.O. (mass%)	BET Surface area (m^2/g)	
					Before dehydration	After dehydration
Goethite ore	355~500	9.02	57.2	24.58	16.58	74.90

CW: Combined water, R.O.: Removable oxygen.

(it is used as a catalyst for some chemical reaction), a sintering of matrix of γ-alumina occurs and a void at the center of particle increases in the elevated temperature. Except for such kind of void, it can be seen that the smaller pores in the matrix were closed by carbon after experiment. The outer area of the particles in Figure 2 is a wax for fixing the sample. It was found that the surface area of samples after experiments (Figures 2(b) and 2(c)) showed a different brightness owing to the difference of carbon density. The width of different color near the surface of sample after 600°C (Figure 2(b)) was about 0.2 mm and that after 800°C was about 0.8 mm. In the case of the sample after 800°C, the width was separated into two regions (Figure 2(c)).

Line analyses of EDS were carried out to determine the distribution of carbon in the γ-alumina along the horizontal lines shown in Figure 2. The results are shown in Figure 3. The carbon distribution of original γ-alumina is lowest and corresponds to a base line of carbon in the EDS analysis. The carbon content of the sample at 600°C was quite

high near the surface about 0.2 mm inside, the content beyond 0.2 mm showed almost the same level. In the case of the sample after 800°C, the width of high carbon content near the surface was thicker and about 0.6 mm to 0.8 mm, which coincided with the SEM observation (Figure 2(c)). These carbon distributions indicated that the carbon bearing species come into the γ-alumina sphere from surface and the carbon precipitated on the surface of pore, which be explained by the mechanism presented by Hüttinger [11] and and Hu et al. [12].

Figure 4 shows the results of XRD for these γ-alumina samples. The peaks of original γ-alumina showed a broad one which meant that the crystalline size was small. When the temperature increased to 600°C and 800°C, each peak became shaper slightly. A broad peak of (002) carbon can be observed around 26° in 2θ, especially at 800°C, which is marked by solid circle (•). The background around 26° at 600°C might mean an existence of carbon, when it was compared with the original γ-alumina. From these results,
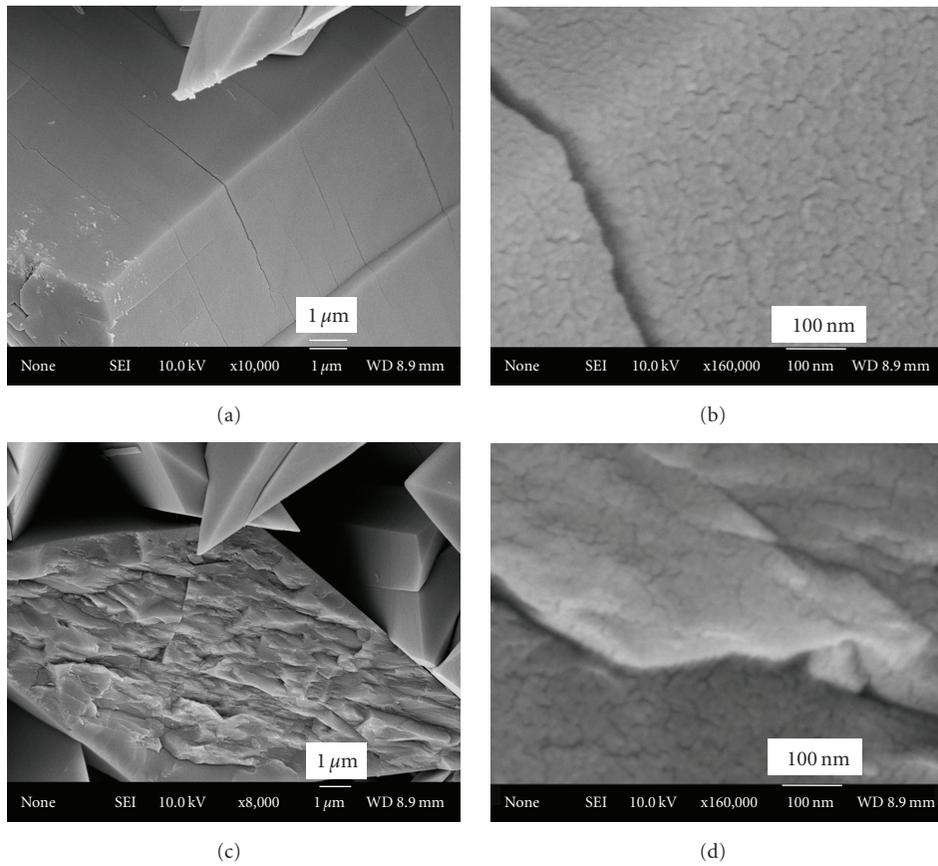
(a)

(b)

(c)

(d)

FIGURE 6: Nanocracks in the Fe_2O_3 formed from Goethite after dehydration at 400°C, (a), (b) side plane and (c), (d) basal plane of orthorhombic (=hexagonal) system.
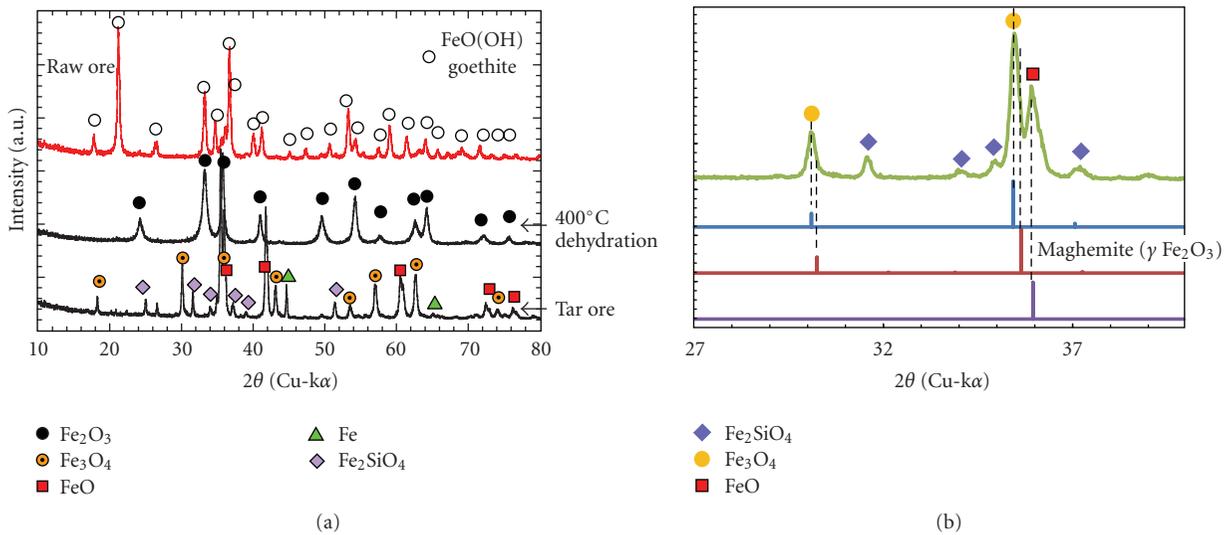

(a)

(b)

FIGURE 7: Comparison of XRD profiles of goethite with/without carbon deposited from tar. (a) Goethite, after dehydration and tar ore, (b) Magnified area in the range from 27° to 40°.
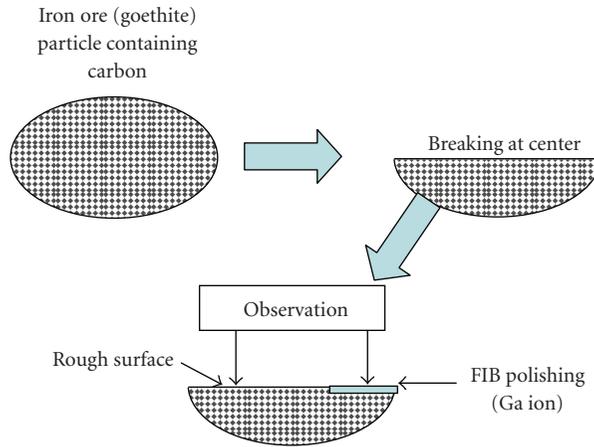
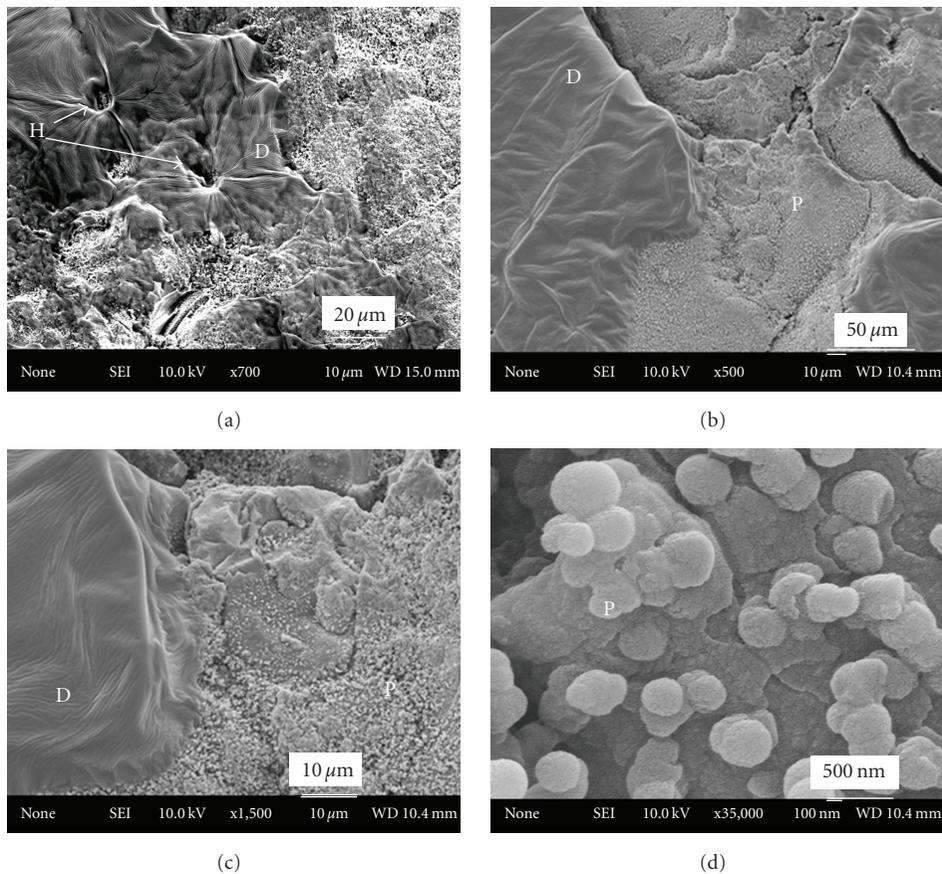FIGURE 8: Preparation of the sample for observation by FE-SEM.

FIGURE 9: Observation of the rough surface by FE-SEM. (D: dense carbon layer, P: particle of carbon in low density).

the crystalline structure of carbon deposited from tar was not so stable and closed to an amorphous one.

3.2. Carbon Deposition in Goethite Ore

3.2.1. Nanocrack Formation after Dehydration of Goethite. As mentioned above, the average pore size obtained by BET was around 4 nm, which is quite small and there was no

direct observation until now. Figure 5 shows the result of FE-SEM observation of the goethite after dehydration. The surface of the sample ore was polished by FIB (focused ion beam) using Ga ion. Figure 5(a) is a photo of low magnification in which the groove made by Ga ion. can be seen Many faceted crystals around 10 μm can be seen under the groove. From the larger magnification photos (Figures 5(b)–5(d)), many orthorhombic crystals exist inside
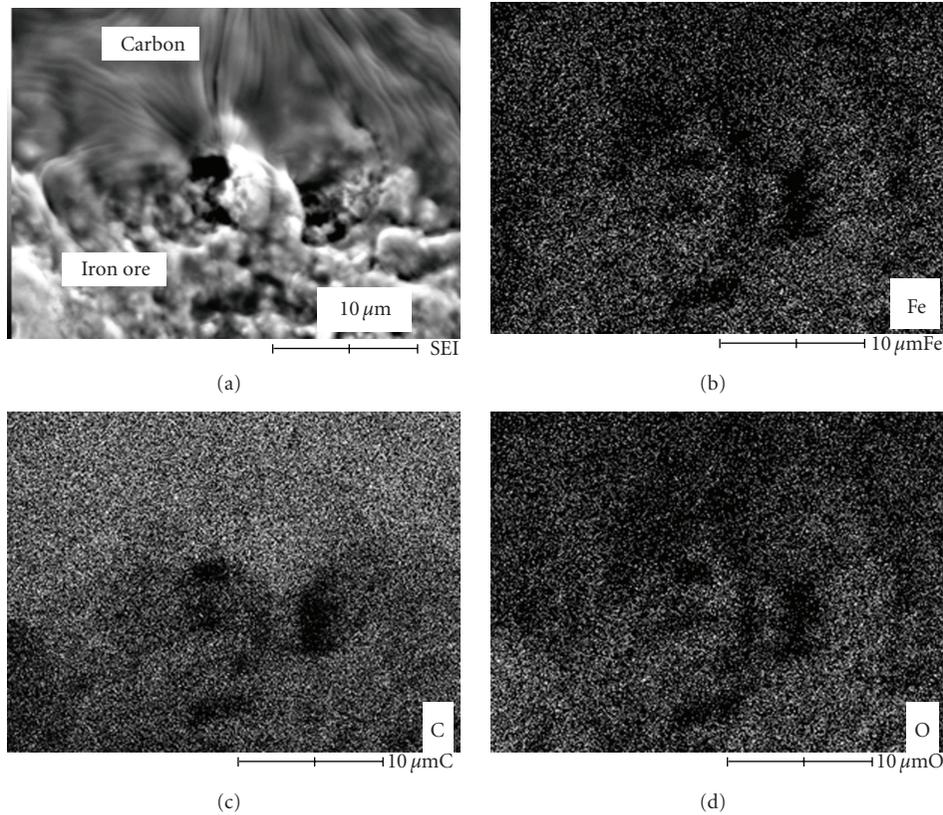
(a)

(b)

(c)

(d)

FIGURE 10: EDS analysis mapping at the edge of the dense carbon layer.

the sample. The goethite is expressed by FeO(OH) and the crystal structure is belonging to the orthorhombic system. And also, the goethite is a cryptocrystalline in Limonite. When the goethite is heated up to 350°C, transformation from FeO(OH) to Fe_2O_3 (hematite) easily occurs as shown by (1). The crystal structure of hematite belongs to hexagonal system which is the same kind of crystal structure

$$2FeO(OH) \longrightarrow Fe_2O_3 + H_2O. \tag{1}$$
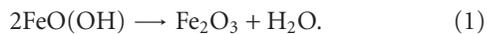
According to H_2O release, a pore or crack will form in the hematite sample. Using FE-SEM, the crystal surface of hematite was observed with ultra-high magnification up to 160,000 times. In this observation, Au film was formed on the surface of hematite crystal by the evaporation method to prevent an electron charge, because the hematite has no electron conductivity. In addition to the Au plating, the sample was fixed on the aluminum holder with silver paste to prevent the image drift and the paste was completely dried for 24 hours under ambient temperature, and then heated up to about 80°C for 2 hours using a dryer. These procedures of sample preparation are important for the observation of ultra-high magnification.

Hu et al. [12] reported the detailed transformation from goethite to hematite in the crystallographic view point. However, in a mesoscopic scale, the size and morphology of void after dehydration is not yet clear. Figures 6(a) and 6(b) show the side plane of hematite crystal after the dehydration

of goethite. There are a number of nanocracks on the side planes of orthorhombic crystals. The dimension of width of cracks is about 4 nm, that it is agreed with the measurement of BET. Furthermore, it was found that the crystalline size was around 20 nm which was a minimum area surrounded by the cracks. Figures 6(c) and 6(d) show the cross section of orthorhombic crystal. The nanocracks were also existing inside the crystal. These cracks have no regularity and no crystallographic orientation. As the hematite unite cell is hexagonal and a = 5.034 Å, c = 13.748 Å, the number of unit cell will be from 20 to 40 in a single crystal, when the crystalline size is assumed to be 20 nm after dehydration.

3.2.2. Carbon Deposition in Hematite Formed from Goethite.
XRD analyses were carried out before and after experiments and the results were shown in Figure 7(a). It can be seen that the original ore is high-purity goethite which was marked with open circle. After dehydration at 400°C, Fe_2O_3 phase was obtained. These XRD patterns mean that the impurities are very low. The term "Tar ore" means that the goethite ore was dehydrated and carbon was deposited from tar in a laboratory experiment. The reduction partially proceeded to the level of metallic iron (Fe) and mainly wustite (FeO or correctly Fe_tO) formed and a magnetite (Fe_3O_4) existed in some portion. In addition, small quantity of fayalite (Fe_2SiO_4) was found after reduction, which meant that the
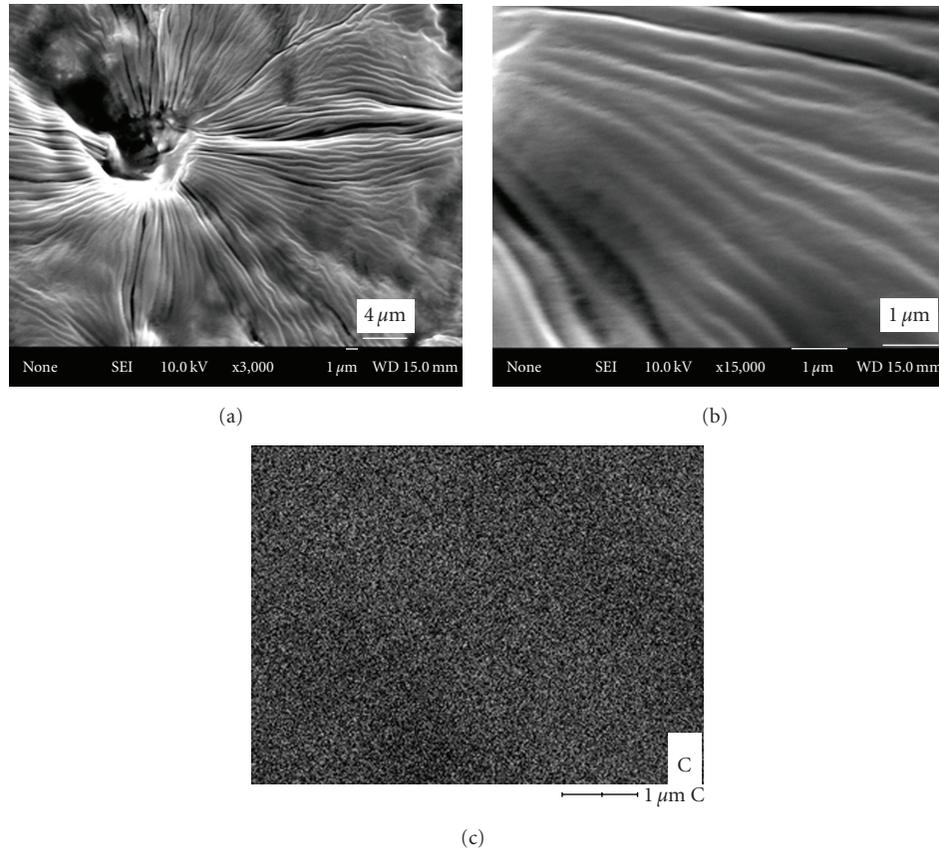
(a)

(b)

(c)

FIGURE 11: Observation and EDS analysis at the dense carbon layer.

relative quantity of the impurity (Fe_2SiO_4) increased after reduction.

Generally, maghemite (γ-Fe_2O_3) is formed by weathering or low-temperature oxidation, while the temperature in this experiment was relatively high. Although it is difficult to distinguish magnetite from maghemite by XRD [11], it is not impossible. Figure 7(b) showed the difference of peak positions between magnetite (Fe_3O_4) and maghemite (γ-Fe_2O_3). From this consideration, it could be concluded that the product in the present experiment was magnetite (Fe_3O_4).

Figure 8 shows the procedures of sample preparation for FE-SEM observation. An ore particle (4-5 mm in diameter) after carbon deposition was broken so as to get a surface within particle. Then, a part of the surface was polished using FIB (focused ion beam) with Ga ion. The observations were performed on both the rough and polished surfaces.

Figure 9 shows the results of FE-SEM observation on the rough surface of sample after carbon deposition. The broken surface was a kind of surface exposed to the gas phase. It might be easily broken at the weakest position like a widely spread crack. The surface was classified into two regions. One is a dense carbon layer, and the other is the surface covered by carbon particles in a low density. These areas are marked "D" and "P", respectively. The dense carbon layers are spread in a radial direction and there is a hole (or a trace of hole) at the center of layer which is marked by "H" in Figure 9(a). The whiter area marked by "P" consists of carbon particles as shown in Figure 9(d).

EDS analysis (JED-2200; detectable from B to U) was performed on the edge of dense carbon layer in Figure 9(a) and the results were shown in Figure 10. The high intensity of characteristic x-ray from carbon element was detected in the area of the dense carbon area, while the intensities of Fe and O elements were relatively higher in the outside of dense layer. From these results, it was concluded that the dense layer consisted of carbon only, and the outside of the dense carbon area was an iron oxide covered by carbon with a lower density.

The observation in high magnification and EDS analysis at the dense carbon layer were performed and the results were shown in Figure 11. The morphology of the surface consisted of lines (plates) with about 0.5 μm in width, which were radially spread. Almost the uniform carbon distribution (Figure 11(c)) was detected in the area of Figure 11(b).

Figure 12 shows the cross section polished by FIB. The surface showed a dappled pattern with dark and bright color where the size of areas was from 0.1 μm to 1 μm. The results of EDS analyses for C, O showed a uniform distribution except a hole. Then, a detailed analysis was performed in higher magnification and the results were shown in Figure 13. As the resolution of EDS analysis is
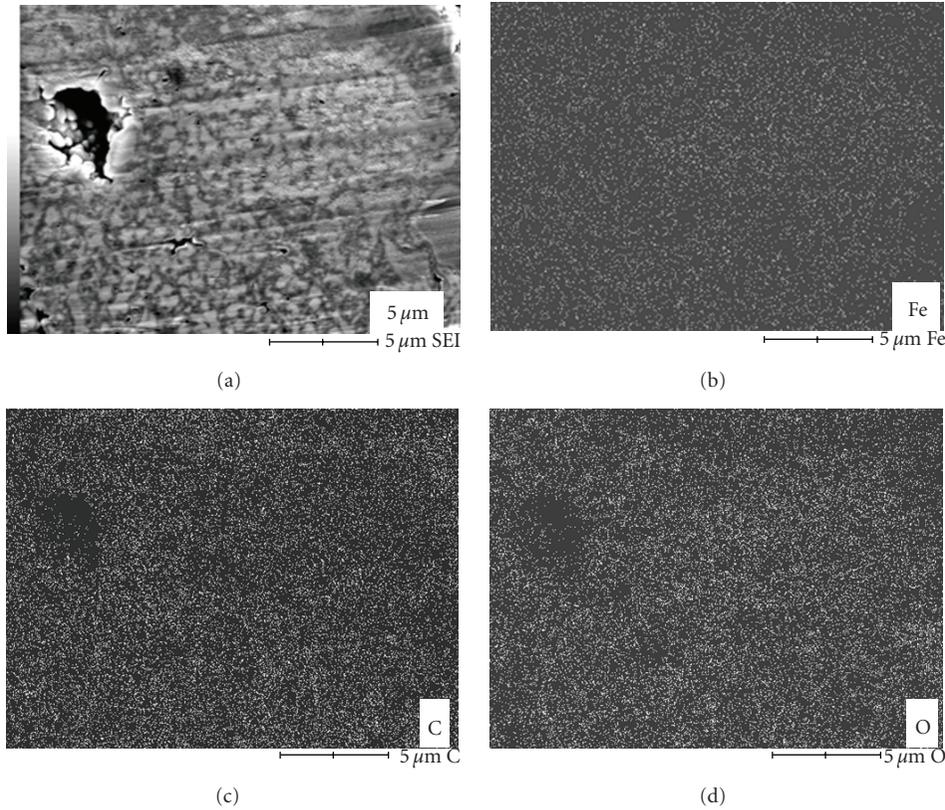
(a)

(b)

(c)

(d)

FIGURE 12: Observation and EDS analysis of the cross section.
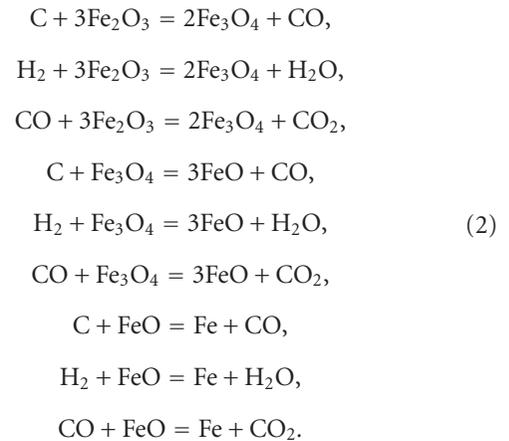
lower than the SEI (secondary electron image) and BEI (back scattered electron image), the element mappings of C and O are ambiguous in this magnification (the mapping of Fe is almost uniform in this area). However, a distribution of C and O elements is slightly understand in Figures 13(b) and 13(c). The outline of the boundaries of the bright and dark areas in Figure 13(a) is emphasized and shown in Figure 13(a'). The emphasized boundaries were again overlapped in the Figures 13(b') and 13(c'). From this operation, it was found that the dark area corresponded to a carbon rich area and the bright area corresponded to a oxygen rich area.

From this observation, it was concluded that the carbon decomposed from tar infiltrated into the nanopore of the hematite and closely infilled; however, since the reduction reaction occurred simultaneously, the original hematite structure might be lost. The mechanism of carbon deposition presented by Hüttinger [11] and Hu et al. [12] is also adequate on this result except for the reduction reaction. Hüttinger's mechanism is shown in Figure 14. They explained their mechanism using CH_4 as a typical hydrocarbon, experimentally and theoretically. The mechanism includes a homogeneous gas phase reaction and a heterogeneous surface reaction of carbon deposition.

In the case of γ-Al_2O_3, there is no need to take into account the reduction reaction. However, the phenomenon of carbon deposition from tar is not fully understood, for example, the precursor of the carbon deposited is not understood exactly. In this study, two possible ways of carbon infiltration are considered: one is tar itself diffusing into the pore and the other is CH_4 decomposed from tar diffusing into the pore which is exactly the same as the mechanism presented by Hüttinger et al. which is illustrated in Figure 15. In case of tar infiltration, although not only H_2 gas but also CO gas might be produced in some content, the CO gas generation is neglected for simplification in Figure 15.

When an iron ore having a number of nanocracks was used for the carbon deposition medium, the reduction reactions occur simultaneously, as shown in Figure 16. The related reactions can be expressed as follows

$$
\begin{aligned}
C + 3Fe_2O_3 &= 2Fe_3O_4 + CO, \\
H_2 + 3Fe_2O_3 &= 2Fe_3O_4 + H_2O, \\
CO + 3Fe_2O_3 &= 2Fe_3O_4 + CO_2, \\
C + Fe_3O_4 &= 3FeO + CO, \\
H_2 + Fe_3O_4 &= 3FeO + H_2O, \quad (2) \\
CO + Fe_3O_4 &= 3FeO + CO_2, \\
C + FeO &= Fe + CO, \\
H_2 + FeO &= Fe + H_2O, \\
CO + FeO &= Fe + CO_2.
\end{aligned}
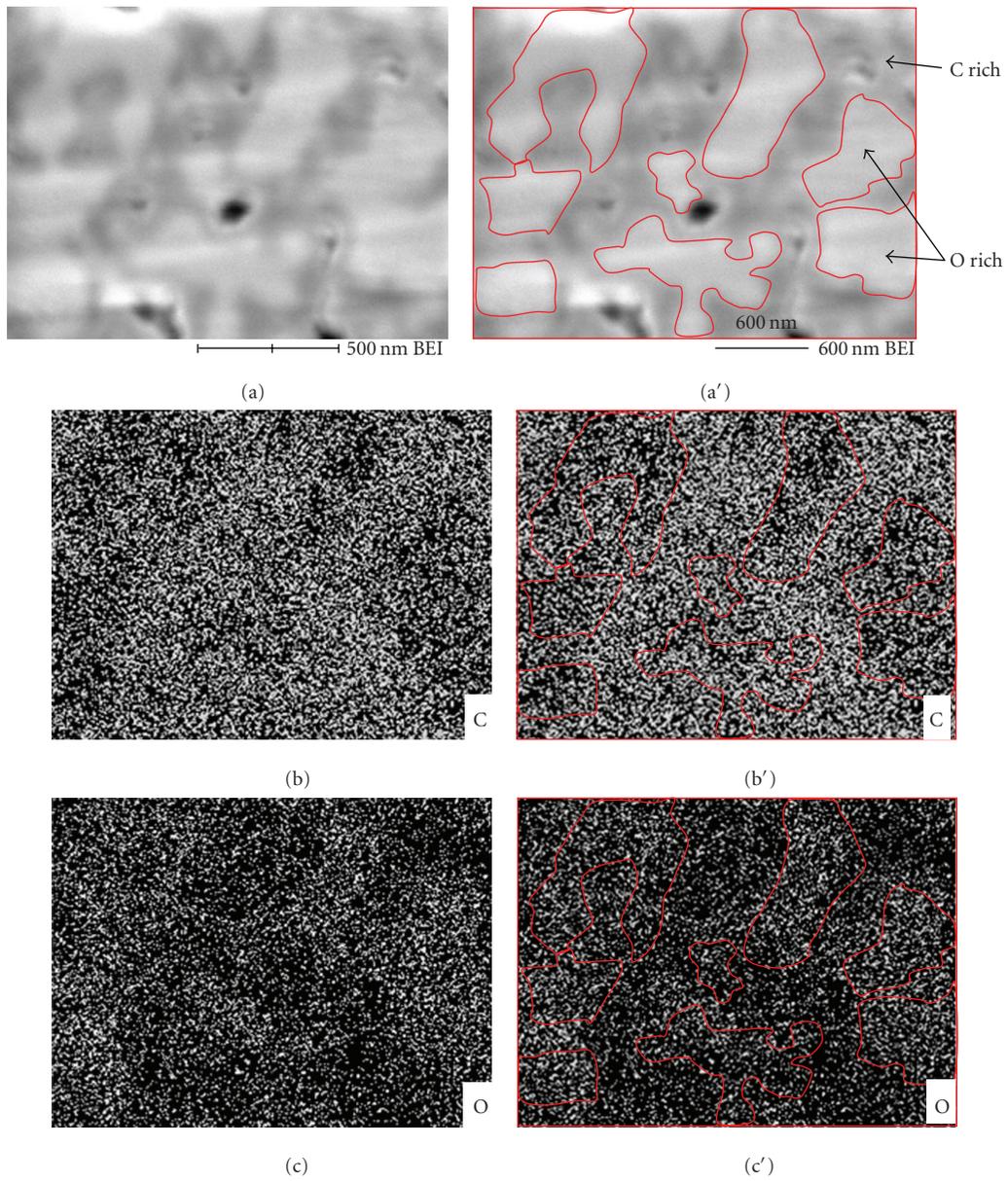$$

(a)
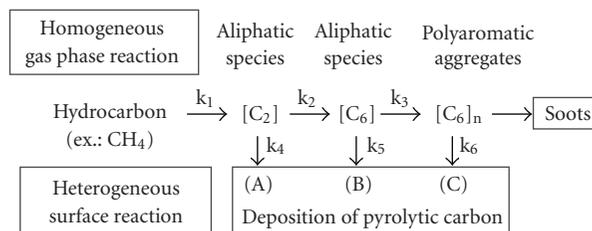
(a′)

(b)

(b′)

(c)

(c′)

FIGURE 13: Difference of C and O content in the microstructure determined by EDS analysis.

By Hüttinger [11]

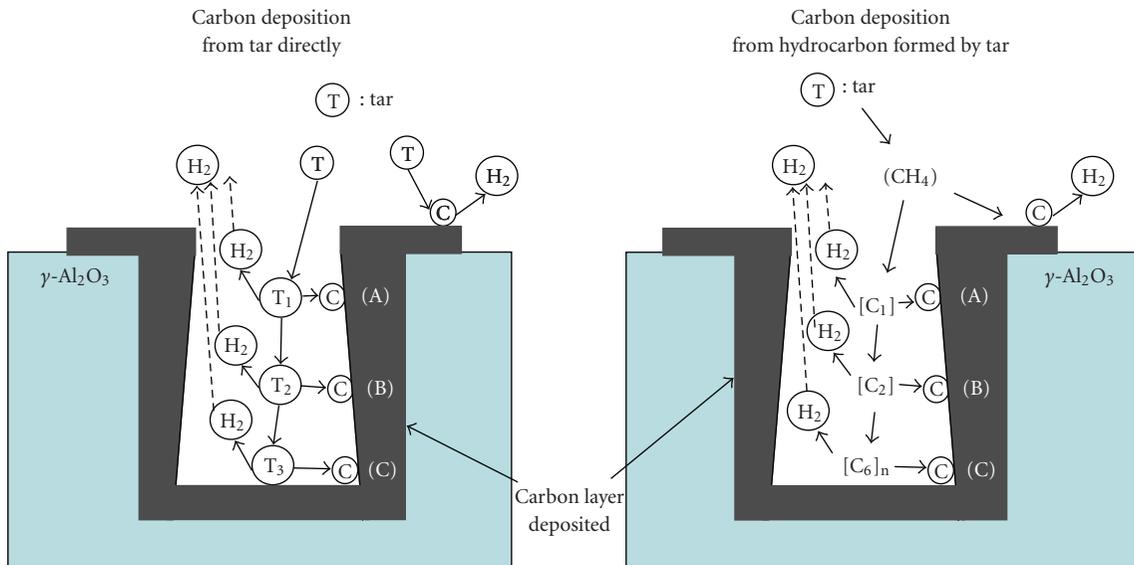FIGURE 14: Mechanism of carbon deposition in a pore from hydrocarbon.

Carbon deposition
from tar directly

Carbon deposition
from hydrocarbon formed by tar

FIGURE 15: Mechanism of carbon deposition in a pore of γ-Al$_2$O$_3$ from tar.

$$C + 3Fe_2O_3 \longrightarrow 2Fe_3O_4 + CO$$
$$H_2 + 3Fe_2O_3 \longrightarrow 2Fe_3O_4 + H_2O$$
$$CO + 3Fe_2O_3 \longrightarrow 2Fe_3O_4 + CO_2$$

$$C + Fe_3O_4 \longrightarrow 3FeO + CO$$
$$H_2 + Fe_3O_4 \longrightarrow 3FeO + H_2O$$
$$CO + Fe_3O_4 \longrightarrow 3FeO + CO_2$$

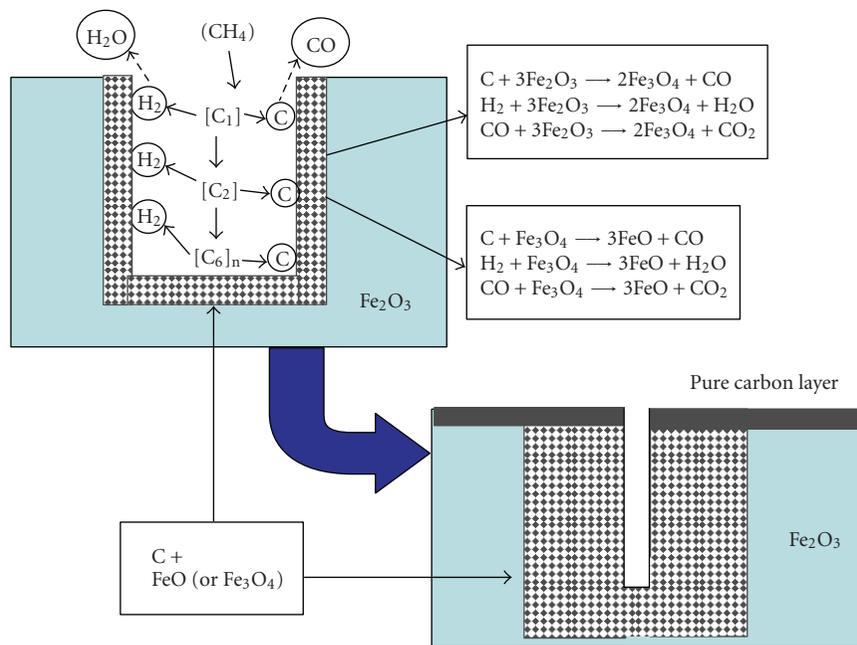$$C + FeO \ (or \ Fe_3O_4)$$

Pure carbon layer

FIGURE 16: Mechanism of carbon deposition and reduction in a crack of Fe$_2$O$_3$ formed from goethite.

The mechanism of the reduction reactions will be complicated, and as shown in Figure 7, various products such as, Fe, FeO, and Fe$_3$O$_4$ were found in the sample. Furthermore, since the experimental temperature was relatively low, reduction did not proceed completely and Fe, O, and C coexisted in the sample. The products will be decided by the reduction reactions (2), and carbon deposition occurred depending on the conditions. Anyway, the rate of carbon deposition would be faster than that of reduction reactions. If the higher reaction temperature was selected, reduction reaction proceeded significantly, and the reaction products would be an iron carbide in addition to metallic iron and carbon.

4. Conclusion

A goethite was dehydrated and a carbon deposition from tar occurred in a nanocracks of hematite. The size and morphology of nanocracks in the hematite formed after dehydration of goethite were clarified by FE-SEM. Furthermore, the distributions and morphologies of the carbon

deposited from tar were investigated. The obtained results are as follows.

(1) The nanocracks formed in the orthorhombic hematite crystals were about 4 nm in width, which is in excellent agreement with the result of BET measurement. The crystalline size surrounded by the cracks was about 20 nm.

(2) When the carbon deposited from tar into the nanocracks, reduction reactions occurred simultaneously. The deposited carbons completely infilled into the nanocracks and the void in the sample.

References

[1] Y. Hata, H. Purwanto, S. Hosokai, J.-I. Hayashi, Y. Kashiwaya, and T. Akiyama, "Biotar ironmaking using wooden biomass and nanoporous iron ore," *Energy and Fuels*, vol. 23, no. 2, pp. 1128–1131, 2009.

[2] T. Sugiyama, M. Saito, H. Uesugi, J. Hayashi, T. Akiyama, and Y. Kashiwaya, "Reduction of low-grade ore by ligneous biomass (Feasibility study of biomass iron making)," *CAMP-ISIJ*, vol. 22, p. 296, 2009.

[3] T. Sugiyama, M. Saito, H. Uesugi, J. Hayashi, T. Akiyama, and Y. Kashiwaya, "Production of ferrous bio-coke by goethite iron ore (Feasibility study of biomass iron making)," *CAMP-ISIJ*, vol. 22, p. 297, 2009.

[4] H. Purwanto, T. Shimada, R. Takahashi, and J.-I. Yagi, "Lowering of grinding energy and enhancement of agglomerate strength by dehydration of Indonesian laterite ore," *ISIJ International*, vol. 42, no. 3, pp. 243–247, 2002.

[5] T. Akiyama, H. Ohta, R. Takahashi, Y. Waseda, and J. Yagi, "Measurement and modeling of thermal conductivity for dense iron oxide and porous iron ore agglomerates in stepwise reduction," *ISIJ International*, vol. 32, no. 7, pp. 829–837, 1992.

[6] C. E. Loo, "Changes in heat transfer when sintering porous goethitic iron ores," *Mineral Processing and Extractive Metallurgy*, vol. 109, pp. C11–C22, 2000.

[7] T. Kawaguchi and T. Usui, "Summarized achievements of the Porous Meso-mosaic Texture Sinter research project," *ISIJ International*, vol. 45, no. 4, pp. 414–426, 2005.

[8] D. C. Goldring and L. M. Juckes, "Iron ore supplies to the United Kingdom iron and steel industry," *Institution of Mining and Metallurgy Transactions A: Mining Technology*, vol. 110, pp. A75–A85, 2001.

[9] A. C. Araujo, S. C. Amarante, C. C. Souza, and R. R. R. Silva, "Ore mineralogy and its relevance for selection of concentration methods in processing of Brazilian iron ores," *Mineral Processing and Extractive Metallurgy*, vol. 112, pp. C54–C64, 2003.

[10] J. Okazaki and K. Higuchi, "Marra Mamba ore, its mineralogical properties and evaluation for utilization," *ISIJ International*, vol. 45, no. 4, pp. 427–435, 2005.

[11] K. J. Hüttinger, "CVD in hot wall reactors—the interaction between homogeneous gas-phase and heterogeneous surface reactions," *Chemical Vapor Deposition*, vol. 4, no. 4, pp. 151–158, 1998.

[12] Z. J. Hu, G. Schoch, and K. J. Hüttinger, "Chemistry and kinetics of chemical vapor infiltration of pyrocarbon. VII: infiltration of capillaries of equal size," *Carbon*, vol. 38, no. 7, pp. 1059–1065, 2000.